Biogenic of CuO nanoparticles using the plant extract Ephedra Alata applied to the removal of methylene blue from wastewater, and its statistical physics analysis

afrah atri
Universite de Monastir Faculte des Sciences de Monastir
Mosaab echabaane (mosaab.echabaane@gmail.com)
Centre de Recherche en Microelectronique et Nanotechnologie https://orcid.org/0000-0001-9230-3815
Mohamed Bouzid
Universite de Monastir Faculte des Sciences de Monastir
Abdelmottaleb Ben Lamine
Universite de Monastir Faculte des Sciences de Monastir
Rafik Ben Chaâbane
Universite de Monastir Institut Preparatoire aux Etudes d'Ingenieur de Monastir

Research Article

Keywords: Biosynthesis, CuO-NPs, Methylene blue, Ephedra Alata, Adsorption, Statistical physics modeling, Wastewater treatment.

Posted Date: April 7th, 2023

DOI: https://doi.org/10.21203/rs.3.rs-2710235/v1

Abstract

Water contaminants due to industrial organic dyes are posing serious human health and environmental problems. Adsorption technology has been widely used in wastewater remediation because of its simplicity, low cost, high effectiveness, and potential to use eco-friendly, non-toxic materials. Herein, the work presents an experimental and theoretical study of the adsorption process of Methylene Blue (MB) dye onto new biogenic copper oxide nanoparticles (CuO NPs) from Ephedra Alata plant extract. The CuO NPs were synthesized via a green chemistry approach and characterized by FE-SEM, EDXS, TEM, XRD, UV–Visible, FTIR, and Raman spectroscopies. The biosynthesized CuO-NPs present a large surface area, nanosize, and a monoclinic structure with phenolic, flavonoid, and hydroxyl groups on the surface. Adsorption tests were carried out under optimal conditions such as pH (7), dye concentration (10 mg/L), and adsorbent dose (0.02 g) to remove the most methylene blue dye from the solution. Adsorption isotherms showed that the capacity of MB adsorbed onto the biosynthesized CuO-NPs increased to 110 and 133.75 mg/g by increasing the temperature to 293 and 323 K, respectively. These experimental data were modeled using statistical physics theory in order to describe the steric and energetic factors involved in the removal of dye, as well as the adsorption mechanism. The modeling analysis demonstrated that MB adsorbed on the CuO-NPs adsorbent surface in a non-parallel orientation. Additionally, the investigated showed the energies of adsorption less than 40 kJ mol^{-1}. According to adsorption energy values, this mechanism progresses by physical adsorption. In summary, green synthesized CuO-NPs are potential materials for organic chemical removal from wastewater treatment.

1. Introduction

Almost two and a half centuries ago, Franklin (1746) cited : "When the Well's dry, we know the worth of water." Now that those wells are at risk of drying up, we are in dire need of pure, fresh water. Due to our egregious abuse of one of our finite and valuable sources, we are to blame for the severe fresh water (drinking) shortage (Khulbe and Matsuura 2018). Because of their acute toxicity and cancer-causing properties, organic contaminants pose a major threat to water quality. In particular, the use of numerous dyes, many of which contain carcinogens and hazardous chemicals, poses a severe threat to the environment and has a negative effect on human health (Vickers 2017). The majority of dyes discharged into the natural water have complex molecular structures and are poisonous, and, hence, challenging to biodegrade (Przystas et al. 2015),(Bedin et al. 2016). The most frequently used dye to color cotton, wood, and silk is methylene blue, a cationic dye (Boukhemkhem and Rida 2017). MB can have several negative effects on human health when consumed in excessive doses, including methemoglobinemia, severe headaches, chest pain, abdominal pain, burning sensations, nausea, vomiting, sweating, and heavy cold sweats.. Additionally, MB may induce respiratory difficulties when inhated (Dhaouadi et al. 2020). The wastewater treatment procedure seeks to minimize the pollutant load to a tolerable level. Common mechanical, biological, or physico-chemical procedures utilized in traditional installations include precipitation, adsorption, electrolysis, coagulation, ion exchange, or oxidation processes. Among this procedures adsorption is the most popular. It is employed all over the world to lessen the various organic pollutants found in wastewater and drinking water systems (Tatarchuk et al. 2020), (Tatarchuk et al. 2019). Moreover, the simplicity of design, performance, cost-effective operation, and efficiency of this adsorption technique have all improved. In addition, The search for the development of new adsorbents that are plentiful, economically lucrative, and successful for treating ecosystems is a big challenge. (Ilgin et al. 2019), (**Lakherwal 2014**), (Malik et al. 2017). Many materials are used as dye adsorbents. Nanoparticles are interesting due to their developed porosity, solubility in a variety of operating fluids, high surface area, excellent chemical and thermal stability, low cost, and practical manufacturing process (Ge et al. 2018), (Sharma et al. 2020). Among the metal oxide nanoparticles, the CuO are p-type group II–VI semiconductors, which have a band gap of 1.2–2.1 eV and monoclinic structures. (Koffyberg and Benko 1982),(Weldegebrieal 2020). Records indicate that the production of metal oxide nanoparticles through physical and chemical processes is increasingly being replaced by biological processes known as biosynthesis or "green synthesis" of nanoparticles because of an innovative, non-toxic, and low-cost method (Vasantharaj et al. 2019), (Pugazhendhi et al. 2018). The biological method of creating metal oxide nanoparticles focuses on using bacterial, yeast, fungal, algal, and plant extracts as reducing agents to create biocompatible nanoparticles that can be made in large quantities (Nasrollahzadeh et al. 2019a), (Nasrollahzadeh et al. 2019b). Due to its simplicity, affordability, and sustainability, the phyto-synthesis of CuONPs using plant extracts has lately attracted increased interest (**Louisiana State** University and Folorunso 2019), (Akintelu et al. 2020). This research, therefore, focuses on the environmentally friendly synthesis of CuO nanoparticles with adsorption capabilities to be utilized as an adsorbent to explore the synergy of adsorption in the elimination of organic contaminants, including its modeling with statistical physics theory.

In this work, we examined the adsorption of MB cationic dyes, an emerging contaminant found in wastewater, using biosynthesized CuO-NPs prepared from Ephedra Alata plant extract. FE-SEM, EDXS, TEM, XRD, UV-Visible, FTIR, and Raman spectroscopies were operated to determine the properties physico-chemical of the of CuO-NPs. MB adsorption on CuO-NPs was carried out under various operating circumstances to examine the effect of temperature on the adsorption process. The experimental data were explained using statistical physics and thermodynamic simulations. According to the modeling outcomes, MB removal using CuO nanoparticles exhibited a synergistic adsorption effect that enhanced removal performance. In addition, the adsorption mechanism of blue methylene was investigated using a monolayer model with two energies based on statistical physics. The method by which MB adsorbed on the created CuO-NPs was investigated using statistical physics. This model was used to analyze how various adsorption systems performed in relation to steric (n_1, n_2, Nm_1 and Nm_2), energetic (C_1 and C_2), and thermodynamic functions. As a result, this work adds novel theoretical discoveries on the mechanism of blue methylene adsorption employing biosynthesized CuO-NPs.

2. Exprimental

2.1. Materials

E. alata plants, also known as alenda locally, were collected in Mednine, Tunisia, and recognised by Mohamed Neffati et al. (Institute of Arid Lands in Mednine, Tunisia). Chemicals of analytical grade were utilized without further purification. Among them was a pentahydrate of copper sulfate ($CuSO_4$,$5H_2O$). Sodium hydroxide (NaOH) and chlorure d'hydrogène (HCl) were used to adjust the pH of the samples. All aqueous solutions were prepared with double-distilled water (DDW). The MB dye was utilized, and Table S1 of the supporting data details its molecular structure.

2.2. Preparation of Green Copper Oxide nanoparticles

An electric mill was used to smash the dry aerial components. The infusion method was used to prepare the extraction. After 45 g of *E. Alata* powder was measured out and placed into Whatman filter sheets, 120 ml of distilled water was added. A brick-red solution was obtained on extraction with water for the week at room temperature. For the synthesis of CuO nanoparticles, 30 ml of *E. alata* extract was extracted and heated at 90°C, and 10 ml of deionized water was combined with 1 g of copper oxide pentahydrate ($CuSO_4.5H_2O$) and stirred at room temperature for 15 minutes. The copper oxide solution was added when the extract's temperature reached 90°C. A magnetic tirrer was used to agitate the liquid for two hours at 90 degrees Celsius. The paste was centrifuged three times for a total of ten minutes at 3500 rpm, followed by a double-distilled water wash. The finished product was dried in a 40°C oven for 24 hours. The CuO nanoparticles were then calcined for 4 hours at 400°C. (Fig. 1).

2.3. Physicochemical characterization of CuO nanoparticles

Different analytical techniques were used to study CuO Nps. The XRD measurements were used out on a Philips X-Pert PRO MPD diffractometer out fitted with a CuK radiation source (λ = 1542 Å). With a step size of 0.02, the difraction patterns were captured in the range of 2 from 30 to 80°. Transmission electron microscopy (TEM) and Field Emission Scanning Electron Microscopy (FE-SEM) methods were utilized to confirm the morphology of CuO-NP. The elemental composition of the samples was analyzed using scanning electron microscopy-energy dispersive X-ray spectroscopy (SEM-EDS), the EDS detector was utilized a Zeiss ULTRA 55 model with an In-Lens SE detector. TEM images were used out using a JEM-100CX2 transmission electron microscope. The optical absorption spectra of CuONps were examined over the wavelength range of 200–800 nm utilizing a UV-Vis SPECORD 210 plus spectrophotometer with a quartz cuvette. FTIR analysis of the extract and CuONPs was performed between 4000 and 400 cm-1. FTIR spectra were captured using KBr pellet disks and a Perkin-Elmer version 5.3 spectrophotometer operating at room temperature. Raman spectroscopy experiments were carried out on a Horiba Jobin Yvon with a spectral resolution of better than 2 cm1 on a Lab Ram HR micro-Raman system combined with a 633 nm wavelength as an excitation source.

2.4. Batch adsorption experiment.

The results of these experiments were used to investigate the effects of dye concentration and temperature on MB adsorption. The adsorption studies were carried out in beakers containing 25 ml of dye solution at a continuous stirring speed of 300 rpm for 24 hours. The effect of three temperatures from 25 to 50°C, different adsorbent dosages from 0.01 to 0.04 g, initial dye concentrations from 5 to 20 mg/l, and pH values (4, 6, 7, 8, and 10) on the adsorption of MB was investigated. The dye concentration was

determined using a UV spectrometer at max = 666 nm. Adsorption capacity (Q_e) and removal percentage (R %) of MB was computed by the following equations:

$$Q_e = \frac{(C_0 - C_t) \times V}{m}$$

1

where C_0 (mg L^{-1}) is the initial concentration, C_t (mg L^{-1}) is the dye concentration at time t, C_e (mg L^{-1}) is the equilibrium concentration in the solution, m is the mass of the CuO catalyst (g) and V is the volume of the solution (L).

2.5. Theoretical adsorption model formalism

To characterize the MB adsorption process on biosynthesized CuO nanoparticles utilizing the statistical physics technique, the receptor site of biosynthesized CuO nanoparticles are taken into account to be either empty or filled by one or more molecules (Lamine and Bouazra 1997), (Bouzid et al. 2019), (Ben Torkia et al. 2018), (**Nakbi et al. 2020**), (Nakbi et al. 2019), (Bouzid et al. 2016b). As there is an interchange of molecules between the adsorbed phase and the liquid phase, the adsorption system is an open system that is best represented by the canonical grand ensemble. The following equation represents the chemical potential of N-dissolved MB molecules and is expressed as follows molecules (Lamine and Bouazra 1997), (Ben Torkia et al. 2018), (**Nakbi et al. 2020**), (Nakbi et al. 2019), (Bouzid et al. 2016b), (Mohamed et al. 2018), (Pang et al. 2020):

$$\mu_m = k_B T \ln\left(\frac{N}{z_{tr}}\right) \qquad (2)$$

Where z_{tr} indicates the partition function of the translation and represents the transition degrees of freedom (Lamine and Bouazra 1997), (Ben Torkia et al. 2018), (**Nakbi et al. 2020**), (Nakbi et al. 2019), (Bouzid et al. 2016b), (Mohamed et al. 2018), (Pang et al. 2020):

$$z_{tr} = V\left(\frac{2\pi m k_B T}{h^2}\right)^{3/2} \qquad (3)$$

V is the volume, *h* is the constant of Planck, *m* is the adsorbed molecule mass, and k_B is the Boltzmann constant. By figuring out the grand canonical partition function, the monolayer model with two types of sites can be expressed as follows (Yazidi et al. 2020), (Li et al. 2020), (Ben Torkia et al. 2020), (Sellaoui et al. 2017), (Ben Torkia et al. 2021), (Bajahzar et al. 2020), (Bel Haj Mohamed et al. 2022):

$$Q_a = \frac{n_1 . N_{m1}}{1 + \left(\frac{C}{C_1}\right)^{n_1}} + \frac{n_2 . N_{m2}}{1 + \left(\frac{C}{C_2}\right)^{n_2}}$$

4

N_{m1} and N_{m2} are the two densities of receptor sites. C_1 and C_2 are the half-saturation concentrations associated to the first and second type of receptor site respectively. n_1 and n_2 are the two numbers of captured molecules per site. The modeling of MB adsorption on biosynthesized CuO nanoparticles is fitted with three model detailed in the Appendix.

3. Resultats And Discussion

3.1. Characterization of biosynthesis CuO nanoparticles

In the SEM images Fig. 1, the green synthesized copper oxide nanoparticles have agglomerated into larger grains. According to the image, only a small number of spherical-shaped particles are synthesized. Most nanoparticles are agglomerated because of the oxidation of metal nanoparticles, while some are quite separated from one another. As a result, nanoparticles of various shapes and sizes perform better in a variety of studies due to their large surfaces and higher reactive sites (Prakash et al. 2018), (Katwal et al. 2015).The TEM findings supported the XRD findings that the synthesized particles were FCC (Ramzan et al. 2021). TEM analysis also showed that the CuO NPs synthesized in green ranged in size from 13 to 40 nm (Fig. 1). By using EDX to identify the elements present in copper oxide nanoparticles, it was confirmed that the copper oxide was pure and free of any other impurities (Fig. 1).

Figure 2 represents the XRD pattern of CuO nanoparticles. In XRD, the peaks with 2θ values of 32.53, 35.46, 35.55, 38.75, 48.70, 53.54, 58.33, 61.55, 66.22, 68.15, 72.42, and 75.04 degrees correspond to crystal planes of (110) (002) (-111) (111) (-202) (020) (202) (-113) (-311) (220) (311) (004) respectively. Unattributed peaks indicate phytochemical compounds, caused by the phenomenon of biocapping, which is common in green synthesis (Ramzan et al. 2021). The angular positions of the peaks and the intensities are in good agreement with the literature and indicate the formation of CuO-NPs (Sharma et al. 2019), (Sundaramurthy and Parthiban 2015). These results confirmed the CuO-NPs' monoclinic structure. The average size of nanocrystals was determined by two methods. The first is Debye Sherrer's formula according to the following equation (Rawat et al. 2020):

$$D = k \times \lambda / \beta \times \cos\theta$$

5

where θ is the Bragg angle, D is the crystallite size (Å), k is a constant of 0.9, λ is the wavelength of the incident X-rays equal to 1.54 Å and β is the width at half peak height (FWHM). The other method is that of Williamson-Hall. This method was estimated by tracing the term cos as a function of 4sin (Singh et al. 2019). The calculated crystallite sizes were 15.21 nm and 21.41 nm, respectively.

Figure 3 displays the absorbance spectrum of CuO-NPs. The extract caused the CuSO4 solution to become green instead of light blue, showing that the copper entity has been reduced to CuO-NPs. The creation of copper oxide nanoparticles was confirmed by the peak absorbance of CuO-NPs, which was detected at 272 nm and is within the range described in the literature (Sahai et al. 2016), (Aksakal and Ciltas 2019), (Angeline Mary et al. 2019). The band gap of the sample was determined by the Tauc formula, which involves plotting $(\alpha h\upsilon)^2$ against hv, as shown in Fig. 3.

$$\alpha h\upsilon = k\left(h\upsilon - E_g\right)^{1/2}$$

6

Where E_g is the direct band gap, hv is the light energy, k is a constant and α is the absorption coefficient. The intersection between the solid lines and the abscissa axis makes it possible to determine E_g which was equal to 1.77 eV.

The FT-IR studies are displayed in Fig. 4. The absorption peaks around 452.3 cm^{-1} corresponded to the stretching vibration and suggested the formation of CuO (Singh et al. 2019), (Angeline Mary et al. 2019). The peaks at 718.49 and 1052.6 cm^{-1} are referred to as the CuO stretching vibrations (Cu-O)(Wang and Pierson 2021). The high peak at 1113.1 cm^{-1} is due to CuO vibrations (Debbichi et al. 2012), while that around 1400 corresponds to phenolic OH bending (Rawat et al. 2020). The bands at about 2898.4 and 2980.5 cm^{-1} are assigned to C-H stretching (Rawat et al. 2020). It has been revealed that phenolic and flavonoid groups are attached to the CuO NPs surface. (Muñoz-Escobar and Reyes-López 2020). The small peak at 3668.7 cm^{-1} is due to hydroxyl groups (Vidovix et al. 2022). As a result, it is demonstrated that several phytochemicals present in the plant extract, including phenols and flavonoides, are involved in the creation of CuO NPs.

Raman spectroscopy is an essential technique for locating the local atomic configurations and vibrations of metal oxides, which aids in identifying the structural properties of micro and nanoparticles. The Raman spectrum of CuO-NPs shown in Fig. 5 revealed three main peaks at 276.6, 320.6, and 604.9 cm^{-1}. As can be seen, there was a low wave number shift compared to bulk CuO-NPs (280,332, and 616). This shift is due to the presence of the plant's extract (Subba Reddy et al. 2018), (**Saruchi. et al. 2019**). The peak at 276.6 cm^{-1} is attributed to the Ag vibrational mode, while the two other peaks at 320.6 and 604.9 cm^{-1} are attributed to the Bg modes. Only the oxygen atoms moved in the Ag and Bg Raman modes, with a dislocation perpendicular to the b-axis for the Bg

modes and in the b-direction for Ag (Mahdavinia et al. 2013), (Naghizade Asl et al. 2016). The nonexistence of peaks associated with other impurities and defects was verified by the absence of Cu_2O and Cu planes in the XRD. According to the Raman spectra, only CuO's XRD patterns can be seen (Ferkous et al. 2022).

3.2. Effect of operational parameter on dye removal

Adsorption is a physical-chemical surface interaction between the adsorbent and the adsorbate. The adsorbents should have favorable surface properties, a large surface area, and a strong mechanical stability for a quick and efficient performance to remove the organic pollutants from the wastewater. The organic pollutants in wastewater act as adsorbates and slowly adsorb on the surface of adsorbents until equilibrium between the adsorbent and adsorbate is reached. The adsorption process was significantly impacted by several variables, such as the pH of the medium, the dye concentration, the temperature, the dosage of the adsorbent, and others.

3.2.1. Effect of initial dye concentration

The effect of the initial dye concentration is in the range of 5–20 mg/L at optimal pH and temperature and fixed number of nanoparticles as illustrated in (**Fig. 6**). The adsorption percentage increased with an increase in the concentration of dye from 5–10 mg/L. After that, the percentage of dye adsorption decreased with increasing initial dye concentrations. As a result, it only slightly favored removal before reaching saturation, mostly because CuO-NP sites and surface areas increased. Due to the saturation of adsorption sites, the maximum adsorption capacity was attained by lowering the adsorbent concentration (Ahmad et al. 2017), (Nandi et al. 2009).

3.2.2. Effect of dose

The rate of adsorption grew as the adsorbent dose increased from 0.01 to 0.04 g at a dye concentration of 10 mg/L, and after reaching its maximum, it began to decrease with subsequent adsorbent dosage increases. This phenomenon could occur due to the increased adsorbent specific surface and the number of vacant sites of adsorbent available for dye cations. As equilibrium was reached, there was a drop in adsorption, which may be attributable to the aggregation or overlapping of adsorption sites (the sites staying saturated), which results in a reduction of the adsorbent surface area available for methylene blue (Rafique et al. 2018). Figure 4 shows the adsorption studies employing 0.02 g of adsorbed material, which results in a dye removal a rate of 96.1%.

3.2.3. Effect of pH

pH is one of the key controlling factors in the adsorption process. It influences the adsorbent's surface charge, the degree of ionization of the adsorbed material, the dissociation of active groups on the adsorbent (Mahdavinia et al. 2013), (Naghizade Asl et al. 2016), and the strength of the electrostatic interactions between the adsorbent and the adsorbate (Ferkous et al. 2022). Therefore, in the current work, the impact of pH was measured by changing pH from 4 to 10 at 25°C. The maximum adsorption was investigated at a fixed dye concentration of 10 mg/L with 20 mg of the nanoparticle dosage. Figures showed the effect of solution pH on the percentage of MB eliminated from the aqueous solution. Based on these findings, pH 7 is the ideal pH for the elimination of MB using CuO NPs created using a green technique. The presence of more OH ions in the solution at this pH (Ahmad et al. 2017), (Nandi et al. 2009) may be responsible for the steady rise in dye removal from polluted water with higher pH (4–10). These OH ions demonstrated greater electrostatic attraction for cationic dye. The change in pH of the solution causes protonation and deprotonation on the surface of the particles, resulting in alterations of charge distribution (Rafique et al. 2018).

3.2.4. Temperature effect

The elimination of MB dye was studied at different temperature values 25, 40 and 50°C, and for different MB dye concentrations (5-300 mg/L), and with a constant adsorbent dose of 0.02g. The adsorption of MB dye rose with the rise of temperature (Fig. 7).

This could be due to the rise of the mobility of MB dye molecules and also to the growth in the pores size of CuO-NPs during the adsorption process. Hence, the adsorption of MB dye was positively impacted by the rise of temperature, indicating that the adsorption mechanism is endothermic in nature (Rafique et al. 2018).

3.3. Statistical physics modeling

The mechanism of MB adsorption by biosynthesized CuO nanoparticles was analyzed using the heterogeneous model with two functional groups (HMTFG). Therefore, the MB adsorption on the biosynthesized CuO nanoparticles was better described with this model than the others. Thus, the modeling results estimated that two types of functional groups on the surface of biosynthesized CuO nanoparticles may participate in the attraction of a non-fixed number of MB molecules. Since, the objective of using this model is to further understand the adsorption mechanism by the analysing of its parameters as a function of temperature. Note that the physicochemical parameters of the HMTFG were defined by steric (n_1, n_2, N_{m1} and N_{m2}) and energetic (C_1 and C_2) variables of the adsorption mechanism.

Table.1 the physicochemical parameters of the HMTFG

T(K)	Q_{1sat} (mg/g)	Q_{2sat} (mg/g)	n_1	n_2	N_{m1} (mg/g)	N_{m2} (mg/g)	C_1 (mg/L)	C_2 (mg/L)	ΔE_1 (kJ/mol)	ΔE_2 (kJ/mol)
298	22.03	105.71	1.71	2.37	12.88	44.60	10.75	140.93	34.68	29.06
313	34.6	117.86	1.54	2.51	22.46	46.95	16.10	164.01	25.92	34.476
323	36.53	117.14	1.42	2.56	25.72	45.75	14.80	146.42	29.01	32.53

3.3.1. Number of captured molecules per functional groups (n_1 and n_2)

The parameter n_i is a stoichiometric coefficient which represents the number of adsorbate molecules captured per functional group (Dhaouadi et al. 2020). It is an important parameter that supplies significant insights into the aggregation phenomenon of MB molecules in the aqueous solution and their orientation on the CuO biosynthesis surface. According to the published articles (Yazidi et al. 2020), (Li et al. 2020), (Ben Torkia et al. 2020), the adsorption orientation of MB can be described by three cases: To suggest an adsorption mechanism, the steric parameters n1 and n2 of the two-energy monolayer model are particularly helpful. Regarding the value of n, there are three conceivable scenarios: n less than 0.5, n between 0.5 and 1, and n greater than 1. The solute's molecules can align on the surface of the adsorbate in two different ways, parallel and non-parallel, with a specific centering for each type of orientation, under the scenario where $0.5 < n < 1$.

- If $n_i<0.5$: this situation indicates that the main functional groups of the CuO biosynthesis can receive a fraction of the MB dye with total parallel orientation (multi-interaction process).
- If $0.5 < n_i<1$: in this case, MB molecules can be adsorbed by the main functional groups with a mixed orientation (% parallel and % non-parallel) implying a multi-molecular adsorption process.
- If $n_i>1$: this third scenario requires that each functional group can capture several molecules simultaneously (non-parallel orientation).

Figure 8 illustrate the variation of this parameter as a function of temperatures. This Fig. 8 indicates that all values of ni (i = 1 and 2) were higher than unity at the tested temperatures, showing that the MB molecules interacted with a non-parallel anchorage with the absorbent surface and each functional group can capture several molecules. This finding also suggests the presence of phenomenon of aggregation of MB molecules in the aqueous solution (monomer, dimer ...) at tested temperatures. Comparatively, the number of molecules captured per functional group follows this trend: n_1 (25°C) < n_2 (25°C), n_1(40°C) < n_2(40°C) and n_1(50°C) < n_2(50°C). It was concluded that the parameter $n_2 > n_1$ at all tested temperatures suggests that the second functional group could play a major role in dye removal.

3.3.2. Densities of occupied receptor sites (N_{m1} and N_{m2})

N_{m1} and N_{m2} are two steric parameters that describe the density of receptor sites. Figure 9 shows the effect of the adsorption temperature on the site density which indicates two different behaviors. The increase in the density of the functional groups of sites 1 (N_{m1}) led to a decrement in the number of sites (n_1) which reflects an increment in the number of anchoring of the dye molecules defined by the inverse of the parameter n (n'= 1/n). The increase of the receptor site density as a function of temperature can be

explained by the presence of additional functional groups that may contribute to the adsorption of MB molecules. Concerning the 2nd site, it can be noted that the increment in the number of sites indicates an increase in the density of occupied sites, which is caused by steric hindrance (Yazidi et al. 2020).

3.3.3. Quantity adsorbed

The parameters Q_{sat1} and Q_{sat2} represent the saturation adsorption capacities related to the first and second sites. They depend on the numbers of captured molecules per adsorption site (n_1,n_2) and the densities of these binding sites (N_{m1},N_{m2}) as $Q_{sat1}=n_1\times N_{m1}$ and $Q_{sat2}=n_2\times N_{m2}$ .Therefore, the total adsorbed quantity is defined by $Q_{total} = Q_{sat1}+Q_{sat2}$. The Fig. 10 shows the results of the adsorbed quantity as a function of temperature. These results showed that the saturation adsorption capacity increased as a function of temperature, which is consistent with the experimental data reflecting that the MB adsorption mechanism was an endothermic process.

Also, the thermal agitation contributed to activating the nanoparticles' surface to making more adsorption sites available for the binding of MB molecules. It was also clear that $Q_{sat1}<Q_{sat2}$, suggesting that the second site played a relatively dominant role in MB removal. It should be remembered that parameters N_m increased with temperature increase. It can be concluded that the saturation adsorption capacity is controlled by the density of occupied sites of the tested adsorbents.

3.3.4. Adsorption energy

Adsorption energies were studied to explain the adsorption mechanism in the system and to characterize the main interactions between MB dye molecules and the surface of copper oxide nanoparticles.
The adsorption energies were calculated with the values of the half-saturation concentrations C_1 and C_2 associated to the two types of adsorption sites at different temperatures by the following equations (Mohamed et al. 2018), (Pang et al. 2020), (Yazidi et al. 2020), (Sghaier et al. 2022), (Bouaziz et al. 2020):

$$\Delta E_1 = -RT.ln\left(\frac{Cs}{C_1}\right)$$

7

$$\Delta E_2 = -RT.ln\left(\frac{Cs}{C_2}\right)$$

8

Where C_1 and C_2 are the half-saturation concentration obtained by adjustments method, Cs is the water solubility of the MB molecules and R = 8.314J/mol.K is the ideal gas constant .

The adsorption energies values are summarized in the **Table 1**. All estimated values were less than 40 kJ/mol, and therefore the MB adsorption process on CuO nanoparticles involves physical interactions in the formation of the adsorbate (MB) layers on the surface of the adsorbent (CuO). Indeed, the positive values of the adsorption energy corresponded to an endothermic adsorption process, which is in agreement with the effect of temperature on the adsorption capacity. Note that the steric parameters, such as the number of sites $n_1 < n_2$, as well as the density of occupied sites $N_{m1}<N_{m2}$ and the quantity of adsorption $Q_{sat1}<Q_{sat2}$, but for energy being the inverse $\Delta E_1 > \Delta E_2$ at all temperatures. This discovery indicates that these steric parameters and the amount of adsorption are the main factors explaining the adsorption of MB dye molecules on CuO nanoparticles; consequently, the adsorption energy did not play a role in the adsorption process in the studied system.

3.3.5. Thermodynamic functions

To determine the interpretation of the adsorption process of dye molecules (MB) on the surface of nanoparticles (CuO), the theory of statistical physics was applied to calculate some thermodynamic potential functions: internal energy, Gibbs free enthalpy and configuration entropy.

- **Internal energy**

Internal energy describes all forms of energy applied to the system. The evolution of the internal energy as a function of the equilibrium concentration for all temperatures is illustrated in Fig. 12.

All negative values of the internal energies were obtained, which confirms that the adsorption system (i.e. the MB and NPs-CuO molecules) evolved spontaneously with energy liberation, resulting in that the adsorption of the MB molecules without any internal contribution. In this context, the increase of the absolute value of the internal energy as a function of temperature is probably due to the increase of the interaction between the MB molecules and the surface of the NPs-CuO and to the increase of the thermal collisions which facilitate the phenomenon of adsorption at high temperature. Moreover, an increase in the concentration was observed, which in turn implies a decrease in the internal energy. In this study, the rise an internal energy represent the amount of work available to introduce the MB molecule in the NPs-CuO nanoparticule receptor sites based adsorbent. The adsorption process was endothermic in nature.

- **Gibbs' enthalpy**

Gibbs' free enthalpy determines the spontaneity of the studied systems. It was provided by the following relation (Bouzid et al. 2016a), (Aouaini et al. 2022), (**Atrous et al**. **2022**).

$$\frac{G_a}{(k_B T)} = \ln\left(\frac{C}{Z_{tr}}\right).\left(\frac{n_1.N_{m1}}{1+\left(\frac{C_1}{C}\right)^{n_1}} + \frac{n_2.N_{m2}}{1+\left(\frac{C_2}{C}\right)^{n_2}}\right)$$

9

According to the Fig. 13, this thermodynamic function was always negative for different temperature values, which indicates that the adsorption process is spontaneous and occurred without external contribution.

Furthermore, the absolute value of the Gibbs enthalpy increases with temperature increase. This is due to the activation phenomenon of the NPs-CuO surface, which results in the activation of the adsorption process becomes endothermic in the course of the temperature, then it believes the spontaneity of the adsorption phenomenon at high temperature. The Gibbs free enthalpy, G_a, was negative, which suggests that the adsorption reaction was spontaneous. This function growth with increasing temperature, which means that the thermal agitation reduced the spontaneity of the adsorption process. The increase of the Gibbs free enthalpy with temperature, $\Delta G_a < 0$, indicates that the adsorption of MB molecules on CuO-systetetized was a thermodynamic spontaneous process Fig. 13. The Gibbs free enthalpy, G_a, increased with the MB concentration and solution temperature and it was confirmed that the adsorption of MB on CuO-systetetized nanoparticules was affected by the thermal agitation effect.

- **Adsorption entropy**

Entropy is a very useful macroscopic quantity, as it describes the order and disorder of MB molecules on the surface of NPs-CuO during the adsorption process and the expression was defined as follows (Bouzid et al. 2016a), (Aouaini et al. 2022), (**Atrous et al**. **2022**):

$$\frac{S_a}{(k_B)} = N_{m1}.\ln\left(1+\left(\frac{C}{C_1}\right)^{n1}\right) - \left(\frac{n_1.\left(\frac{C}{C_1}\right)^{n1}.\ln\left(\frac{C}{C_1}\right)}{1+\left(\frac{C_1}{C}\right)^{n_1}}\right) + N_{m2}.\ln\left(1+\left(\frac{C}{C_2}\right)^{n2}\right) - \left(\frac{n_2.\left(\frac{C}{C_2}\right)^{n2}.\ln\left(\frac{C}{C_2}\right)}{1+\left(\frac{C_2}{C}\right)^{n2}}\right)$$

10

Figure 14 shows the evolution of entropy as a function of concentration at different temperatures. Entropy has two different behaviors.

First, at low concentrations, entropy increases with equilibrium concentration, so the disorder also increased. This is because MB molecules had a strong possibility to choose and find a vacant receptor site and then an empty NP surface. This is due to the availability of many receptor sites on the surface of the nanoparticles (CuO) based adsorbent. Therefore, the MB molecules were connecting the empty sites. Then, at high concentration, the entropy configuration decreased. This reduction is due to the decrease

in the number of free sites. Then, the disorder decreased with the increase of the concentration which limited the number of possible configurations because the vacant sites were limited and consequently the decrement of the entropy since the surface of the NPs tended to saturation and therefore towards order. The evolution of confgurational entropy (S_a) showed one stationary point corresponding to the two-half saturation concentrations C_1 and C_2 where the disorder was maximum when half of the density of adsorption sites (N_{m1} and N_{m2}) on CuO-synthetised nanoparticales surface were occupied.

4. Conclusion

In this work, plant extract from the E. alata species was used in the green production of copper oxide nanoparticles. Phytochemicals included in the plant extract serve as reducing, capping, and stabilizing agents, effectively converting copper metal ions into CuO-NPs. The physicochemical properties of ZnO NPs were successfully studied using FE-SEM, EDXS, TEM, XRD, UV–Visible, FTIR, and Raman spectroscopy measurements. The characterization revealed that the nanoparticles were oxidized, demonstrating the effectiveness of the plant extract-based green synthesis. The synthesized CuO-NPs were effectively used to lessen the methylene blue (MB) dye's harmful effects in wastewater bodies, and they were further optimized under various experimental conditions. Maximum MB removal was obtained at equilibrium with pH 7, adsorbent dose (0.02 g) and adsorbate concentration (10 mg/L). The maximum adsorption capacity was 133.75 mg/g at 323 K. To examine the energetic and steric parameters of the MB adsorption on the nanoparticle surface, statistical physics calculations were performed using a monolayer model. It was discovered that, where multi-molecular adsorption was anticipated, this adsorption process was primarily controlled by electrostatic interactions and hydrogen bonds. Thermodynamic investigations revealed the biosorption process to be an endothermic, spontaneous, and reversible process. According to the results of this study, CuO nanoparticles with high dye adsorption capacities might be a good choice for removing colored dyes from aqueous solutions.

Declarations

Ethical Approval:

Not applicable for this study.

Consent to Participate:

Not applicable for this study.

Consent to Publish:

All authors consent to this publication.

Competing Interests:

The authors declare no competing interests.

Availability of data and materials

Data and materials are contained within the article.

Funding:

This work was supported by Tunisian’s Ministry of high education and scientific research.

Authors Contribution:

Afrah Atri: writing-original draft, visualization, conceptualization, methodology. Mosaab Echabaane: visualization, writing-review and editing; conceptualization, methodology. Mohamed Bouzid : resources, writing-review and editing. Abdelmottaleb Ben Lamine: writing-reviewing and editing. Rafik Ben Chaâbane: writing-reviewing and editing, visualization, supervision.

References

1. Thakur S, Kumar P V (2019) Kinetics and thermodynamic studies for removal of methylene blue dye by biosynthesize copper oxide nanoparticles and its antibacterial activity. J Environ Health Sci Engineer 17:367–376. https://doi.org/10.1007/s40201-019-00354-1
2. Ahmad I, Akhtar MJ, Jadoon IBK et al (2017) Equilibrium modeling of cadmium biosorption from aqueous solution by compost. Environ Sci Pollut Res 24:5277–5284. https://doi.org/10.1007/s11356-016-8280-y
3. Akintelu SA, Folorunso AS, Folorunso FA, Oyebamiji AK (2020) Green synthesis of copper oxide nanoparticles for biomedical application and environmental remediation. Heliyon 6:e04508. https://doi.org/10.1016/j.heliyon.2020.e04508
4. Aksakal FI, Ciltas A (2019) Impact of copper oxide nanoparticles (CuO NPs) exposure on embryo development and expression of genes related to the innate immune system of zebrafish (Danio rerio). Comp Biochem Physiol C: Toxicol Pharmacol 223:78–87. https://doi.org/10.1016/j.cbpc.2019.05.016
5. Angeline Mary AP, Thaminum Ansari A, Subramanian R (2019) Sugarcane juice mediated synthesis of copper oxide nanoparticles, characterization and their antibacterial activity. J King Saud Univ - Sci 31:1103–1114. https://doi.org/10.1016/j.jksus.2019.03.003
6. Aouaini F, Bouzgarou S, Bouzid M et al (2022) CO2 adsorption by molecular sieve 10A°, experimental and theoretical examination via statistical physics: modeling macroscopic and microscopic investigation. Sep Sci Technol 57:2532–2542. https://doi.org/10.1080/01496395.2022.2080708
7. Bajahzar A, Bouzid M, Briki C et al (2020) Experimental and numerical study of the isotherms and determination of physicochemical parameters of the hydrogen absorption/desorption process by the metal hydrides. Int J Hydrog Energy 45:15281–15293. https://doi.org/10.1016/j.ijhydene.2020.04.016
8. Bedin KC, Martins AC, Cazetta AL et al (2016) KOH-activated carbon prepared from sucrose spherical carbon: Adsorption equilibrium, kinetic and thermodynamic studies for Methylene Blue removal. Chem Eng J 286:476–484. https://doi.org/10.1016/j.cej.2015.10.099
9. Bel Haj Mohamed N, Ouni S, Bouzid M et al (2022) Synthesis and preparation of acid capped CdSe nanocrystals as successful adsorbent and photocatalyst for the removal of dyes from water and its statistical physics analysis. Environ Sci Pollut Res 29:72747–72763. https://doi.org/10.1007/s11356-022-20990-9
10. Ben Torkia Y, Atrous M, Bouzid M et al (2020) Stereographic and energetic studies of acid blue 9 adsorption onto Spirulina platensis (strain LEB-52) based on statistical physics approach. Chem Eng Commun 207:445–457. https://doi.org/10.1080/00986445.2019.1604513
11. Ben Torkia Y, Dotto GL, Ben Lamine A (2018) Statistical physics modeling of synthetic dyes adsorption onto Spirulina platensis nanoparticles. Environ Sci Pollut Res 25:28973–28984. https://doi.org/10.1007/s11356-018-2898-x
12. Ben Torkia Y, Sghaier W, Bouzid M et al (2021) Adsorption of acetylene on exfoliated graphite surface: energetic and stereographic studies by applying statistical physics treatment. Sep Sci Technol 56:2578–2586. https://doi.org/10.1080/01496395.2020.1837875
13. Bouaziz N, Ben Manaa M, Bouzid M, Ben Lamine A (2020) Adsorption of hydrogen in defective carbon nanotube: modelling and consequent investigations using statistical physics formalism. Mol Phys 118:e1606460. https://doi.org/10.1080/00268976.2019.1606460
14. Boukhemkhem A, Rida K (2017) Improvement adsorption capacity of methylene blue onto modified Tamazert kaolin. Adsorpt Sci Technol 35:753–773. https://doi.org/10.1177/0263617416684835
15. Bouzid M, Bouaziz N, Torkia YB, Lamine AB (2019) Statistical physics modeling of ethanol adsorption onto the phenol resin based adsorbents: Stereographic, energetic and thermodynamic investigations. J Mol Liq 283:674–687. https://doi.org/10.1016/j.molliq.2019.03.129

16. Bouzid M, Nasri F, Belmabrouk H (2016a) Numerical Study of Electro-Chemical System for Enzymatic Activities Detection. Sens Lett 14:1079–1083. https://doi.org/10.1166/sl.2016.3730
17. Bouzid M, Sellaoui L, Khalfaoui M et al (2016b) Adsorption of ethanol onto activated carbon: Modeling and consequent interpretations based on statistical physics treatment. Physica A 444:853–869. https://doi.org/10.1016/j.physa.2015.09.097
18. Debbichi L, Marco de Lucas MC, Pierson JF, Krüger P (2012) Vibrational Properties of CuO and Cu4O3 from First-Principles Calculations, and Raman and Infrared Spectroscopy. J Phys Chem C 116:10232–10237. https://doi.org/10.1021/jp303096m
19. Dhaouadi F, Sellaoui L, Dotto GL et al (2020) Adsorption of methylene blue on comminuted raw avocado seeds: Interpretation of the effect of salts via physical monolayer model. J Mol Liq 305:112815. https://doi.org/10.1016/j.molliq.2020.112815
20. Ferkous H, Rouibah K, Hammoudi N-E-H et al (2022) The Removal of a Textile Dye from an Aqueous Solution Using a Biocomposite Adsorbent. Polymers 14:2396. https://doi.org/10.3390/polym14122396
21. Ge L, Wang W, Peng Z et al (2018) Facile fabrication of Fe@MgO magnetic nanocomposites for efficient removal of heavy metal ion and dye from water. Powder Technol 326:393–401. https://doi.org/10.1016/j.powtec.2017.12.003
22. Ilgin P, Ozay H, Ozay O (2019) Selective adsorption of cationic dyes from colored noxious effluent using a novel N-tert-butylmaleamic acid based hydrogels. Reactive and Functional Polymers 142:189–198. https://doi.org/10.1016/j.reactfunctpolym.2019.06.018
23. Katwal R, Kaur H, Sharma G et al (2015) Electrochemical synthesized copper oxide nanoparticles for enhanced photocatalytic and antimicrobial activity. J Ind Eng Chem 31:173–184. https://doi.org/10.1016/j.jiec.2015.06.021
24. Khulbe KC, Matsuura T (2018) Removal of heavy metals and pollutants by membrane adsorption techniques. Appl Water Sci 8:19. https://doi.org/10.1007/s13201-018-0661-6
25. Koffyberg FP, Benko FA (1982) A photoelectrochemical determination of the position of the conduction and valence band edges of p-type CuO. J Appl Phys 53:1173–1177. https://doi.org/10.1063/1.330567
26. Lakherwal D Adsorption of Heavy Metals: A Review. 8
27. Lamine AB, Bouazra Y (1997) Application of Statistical Thermodynamics to the Olfaction Mechanism. Chem Senses 22:67–75. https://doi.org/10.1093/chemse/22.1.67
28. Li Z, Sellaoui L, Gueddida S et al (2020) Adsorption of methylene blue on silica nanoparticles: Modelling analysis of the adsorption mechanism via a double layer model. J Mol Liq 319:114348. https://doi.org/10.1016/j.molliq.2020.114348
29. University LS, Folorunso AS (2019) Characterization And Antimicrobial Investigation Of Synthesized Silver Nanoparticles From Annona Muricata Leaf Extracts. NTMB 6:1–5. https://doi.org/10.24966/NTMB-2044/100022
30. Mahdavinia GR, Aghaie H, Sheykhloie H et al (2013) Synthesis of CarAlg/MMt nanocomposite hydrogels and adsorption of cationic crystal violet. Carbohydr Polym 98:358–365. https://doi.org/10.1016/j.carbpol.2013.05.096
31. Malik DS, Jain CK, Yadav AK (2017) Removal of heavy metals from emerging cellulosic low-cost adsorbents: a review. Appl Water Sci 7:2113–2136. https://doi.org/10.1007/s13201-016-0401-8
32. Mohamed B, Qingyu Z, Moggridge D, Abdelmottaleb G BL (2018) New insight in adsorption of pyridine on the two modified adsorbents types MN200 and MN500 by means of grand canonical ensemble. J Mol Liq 263:413–421. https://doi.org/10.1016/j.molliq.2018.05.008
33. Muñoz-Escobar A, Reyes-López SY (2020) Antifungal susceptibility of Candida species to copper oxide nanoparticles on polycaprolactone fibers (PCL-CuONPs). PLoS ONE 15:e0228864. https://doi.org/10.1371/journal.pone.0228864
34. Naghizade Asl M, Mahmodi NM, Teymouri P et al (2016) Adsorption of organic dyes using copper oxide nanoparticles: isotherm and kinetic studies. Desalination Water Treat 57:25278–25287. https://doi.org/10.1080/19443994.2016.1151832
35. Nakbi A, Bouzid M, Ayachi F et al (2019) Investigation of caffeine taste mechanism through a statistical physics modeling of caffeine dose-taste response curve by a biological putative caffeine adsorption process in electrophysiological response. Prog Biophys Mol Biol 149:70–85. https://doi.org/10.1016/j.pbiomolbio.2018.12.013
36. Nandi BK, Goswami A, Purkait MK (2009) Removal of cationic dyes from aqueous solutions by kaolin: Kinetic and equilibrium studies. Appl Clay Sci 42:583–590. https://doi.org/10.1016/j.clay.2008.03.015
37. Nasrollahzadeh M, Ghorbannezhad F, Issaabadi Z, Sajadi SM (2019a) Recent Developments in the Biosynthesis of Cu-Based Recyclable Nanocatalysts Using Plant Extracts and their Application in the Chemical Reactions. Chem Record 19:601–643. https://doi.org/10.1002/tcr.201800069

38. Nasrollahzadeh M, Mahmoudi-Gom Yek S, Motahharifar N, Ghafori Gorab M (2019b) Recent Developments in the Plant-Mediated Green Synthesis of Ag-Based Nanoparticles for Environmental and Catalytic Applications. Chem Record 19:2436–2479. https://doi.org/10.1002/tcr.201800202
39. Pang X, Bouzid M, dos Santos JMN et al (2020) Theoretical study of indigotine blue dye adsorption on CoFe2O4/chitosan magnetic composite via analytical model. Colloids Surf A 589:124467. https://doi.org/10.1016/j.colsurfa.2020.124467
40. Prakash S, Elavarasan N, Venkatesan A et al (2018) Green synthesis of copper oxide nanoparticles and its effective applications in Biginelli reaction, BTB photodegradation and antibacterial activity. Adv Powder Technol 29:3315–3326. https://doi.org/10.1016/j.apt.2018.09.009
41. Przystas W, Zablocka-Godlewska E, Grabinska-Sota E (2015) Efficacy of fungal decolorization of a mixture of dyes belonging to different classes. Braz J Microbiol 46:415–424. https://doi.org/10.1590/S1517-838246246220140167
42. Pugazhendhi A, Kumar SS, Manikandan M, Saravanan M (2018) Photocatalytic properties and antimicrobial efficacy of Fe doped CuO nanoparticles against the pathogenic bacteria and fungi. Microb Pathog 122:84–89. https://doi.org/10.1016/j.micpath.2018.06.016
43. Rafique M, Shaikh AJ, Rasheed R et al (2018) Aquatic Biodegradation of Methylene Blue by Copper Oxide Nanoparticles Synthesized from Azadirachta indica Leaves Extract. J Inorg Organomet Polym 28:2455–2462. https://doi.org/10.1007/s10904-018-0921-9
44. Ramzan M, Obodo RaphaelM, Mukhtar S et al (2021) Green synthesis of copper oxide nanoparticles using Cedrus deodara aqueous extract for antibacterial activity. Materials Today: Proceedings 36:576–581. https://doi.org/10.1016/j.matpr.2020.05.472
45. Rawat P, Nigam A, Kala S (2020) Green synthesis of copper and copper sulfide nanoparticles. AIP Conference Proceedings 2220:020102. https://doi.org/10.1063/5.0001319
46. Sahai A, Goswami N, Kaushik SD, Tripathi S (2016) Cu/Cu2O/CuO nanoparticles: Novel synthesis by exploding wire technique and extensive characterization. Appl Surf Sci 390:974–983. https://doi.org/10.1016/j.apsusc.2016.09.005
47. Sellaoui L, Soetaredjo FE, Ismadji S et al (2017) New insights into single-compound and binary adsorption of copper and lead ions on a treated sea mango shell: experimental and theoretical studies. Phys Chem Chem Phys 19:25927–25937. https://doi.org/10.1039/C7CP03770H
48. Sghaier W, Ben Torkia Y, Bouzid M, Ben Lamine A (2022) Thermodynamic analysis of cooling cycles based on statistical physics modeling of ethanol adsorption isotherms. Int J Refrig 141:119–131. https://doi.org/10.1016/j.ijrefrig.2022.05.022
49. Sharma M, Poddar M, Gupta Y et al (2020) Solar light assisted degradation of dyes and adsorption of heavy metal ions from water by CuO–ZnO tetrapodal hybrid nanocomposite. Mater Today Chem 17:100336. https://doi.org/10.1016/j.mtchem.2020.100336
50. Sharma P, Pant S, Dave V et al (2019) Green synthesis and characterization of copper nanoparticles by Tinospora cardifolia to produce nature-friendly copper nano-coated fabric and their antimicrobial evaluation. J Microbiol Methods 160:107–116. https://doi.org/10.1016/j.mimet.2019.03.007
51. Singh J, Kumar V, Kim K-H, Rawat M (2019) Biogenic synthesis of copper oxide nanoparticles using plant extract and its prodigious potential for photocatalytic degradation of dyes. Environ Res 177:108569. https://doi.org/10.1016/j.envres.2019.108569
52. Subba Reddy Y, Maria Magdalane C, Kaviyarasu K et al (2018) Equilibrium and kinetic studies of the adsorption of acid blue 9 and Safranin O from aqueous solutions by MgO decked FLG coated Fuller's earth. J Phys Chem Solids 123:43–51. https://doi.org/10.1016/j.jpcs.2018.07.009
53. Sundaramurthy N, Parthiban C (2015) Biosynthesis of copper oxide nanoparticles using Pyrus pyrifolia leaf extract and evolve the catalytic activity. Int Res J Eng Technol 2:332–338
54. Tatarchuk T, Myslin M, Mironyuk I et al (2020) Synthesis, morphology, crystallite size and adsorption properties of nanostructured Mg–Zn ferrites with enhanced porous structure. J Alloys Compd 819:152945. https://doi.org/10.1016/j.jallcom.2019.152945
55. Tatarchuk T, Shyichuk A, Mironyuk I, Naushad Mu (2019) A review on removal of uranium(VI) ions using titanium dioxide based sorbents. J Mol Liq 293:111563. https://doi.org/10.1016/j.molliq.2019.111563

56. Vasantharaj S, Sathiyavimal S, Saravanan M et al (2019) Synthesis of ecofriendly copper oxide nanoparticles for fabrication over textile fabrics: Characterization of antibacterial activity and dye degradation potential. J Photochem Photobiol B 191:143–149. https://doi.org/10.1016/j.jphotobiol.2018.12.026
57. Vickers NJ (2017) Animal Communication: When I'm Calling You, Will You Answer Too? Curr Biol 27:R713–R715. https://doi.org/10.1016/j.cub.2017.05.064
58. Vidovix TB, Quesada HB, Bergamasco R et al (2022) Adsorption of Safranin-O dye by copper oxide nanoparticles synthesized from *Punica granatum* leaf extract. Environ Technol 43:3047–3063. https://doi.org/10.1080/09593330.2021.1914180
59. Wang Y, Pierson JF (2021) Binary copper oxides as photovoltaic absorbers: recent progress in materials and applications. J Phys D: Appl Phys 54:263002. https://doi.org/10.1088/1361-6463/abf165
60. Weldegebrieal GK (2020) Photocatalytic and antibacterial activityof CuO nanoparticles biosynthesized using Verbascum thapsus leaves extract. Optik 204:164230. https://doi.org/10.1016/j.ijleo.2020.164230
61. Yazidi A, Sellaoui L, Badawi M et al (2020) Ternary adsorption of cobalt, nickel and methylene blue on a modified chitin: Phenomenological modeling and physical interpretation of the adsorption mechanism. Int J Biol Macromol 158:595–604. https://doi.org/10.1016/j.ijbiomac.2020.05.022
62. Quantitative characterization of sucrose taste by statistical physics modeling parameters using an analogy between an experimental physicochemical isotherm of sucrose adsorption on β-cyclodextrin and a putative biological sucrose adsorption from sucrose dose-taste response curve (psychophysics and electrophysiology) - ScienceDirect. https://www.sciencedirect.com/science/article/pii/S0167732219320288. Accessed 5 Mar 2023a
63. Statistical physics treatment of tetracycline adsorption: energetic studies | SpringerLink. https://link.springer.com/article/10.1007/s11696-022-02171-7. Accessed 5 Mar 2023b

Figures

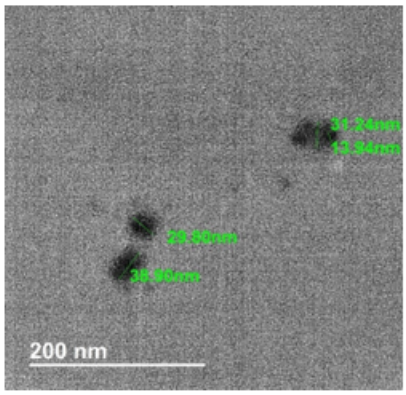

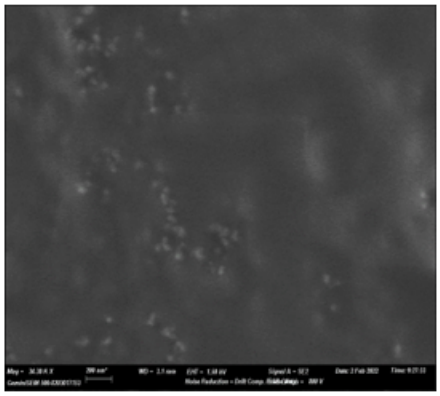

Element	Wt%	Wt% Sigma	Atomic %	Standard Label	Factory Standard
C	4,99	0,13	14,73	C Vit	Yes
O	19,5	0,13	43,18	SiO2	Yes
Cu	75,5	0,17	42,09	Cu	Yes
Total:	100		100		

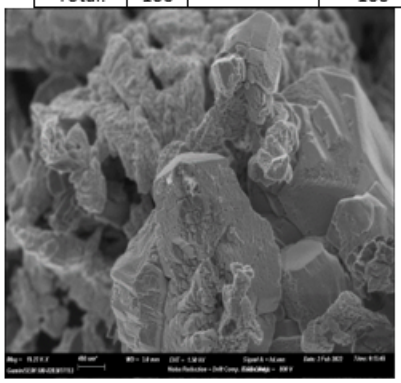

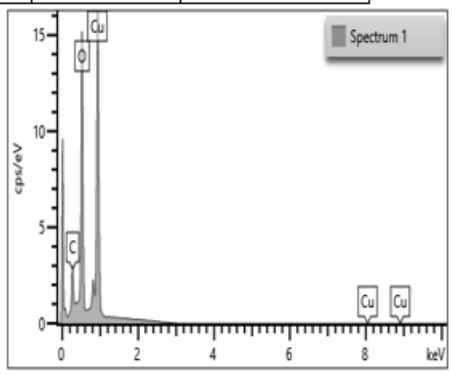

Figure 1

FE-SEM images and EDX profile of CuO biosynthesized nanoparticles

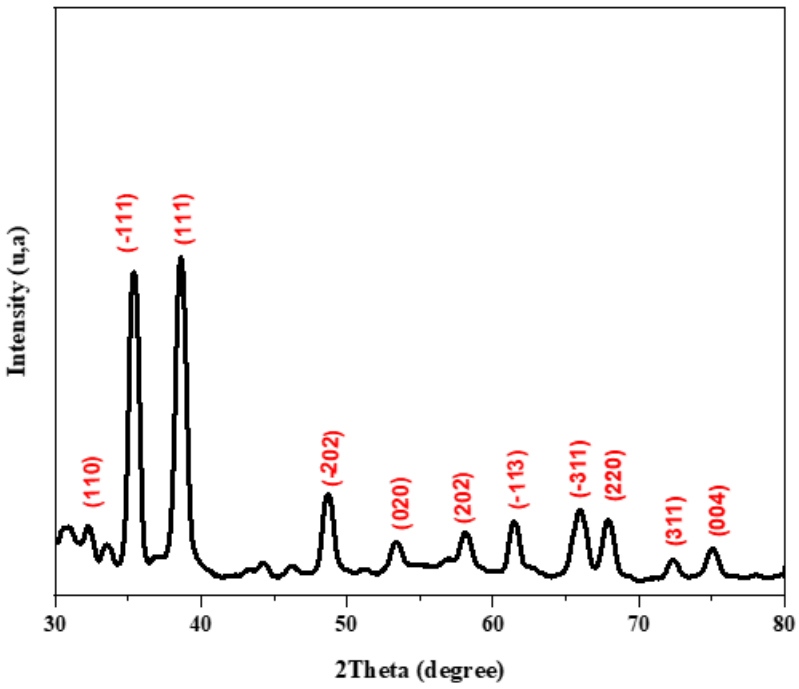

Figure 2

XRD patterns of CuO-NPs

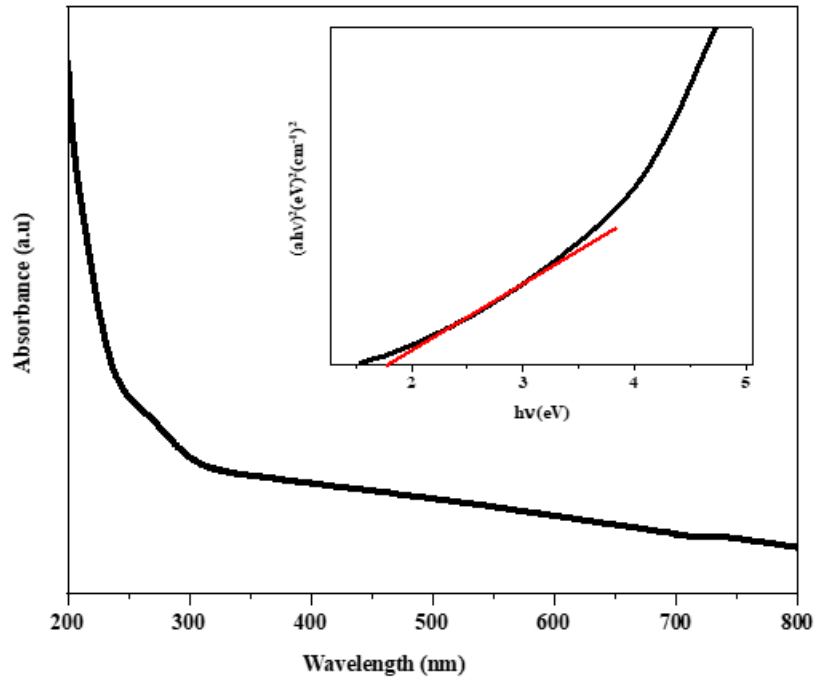

Figure 3

UV-Visible absorption spectra of CuO-NPs

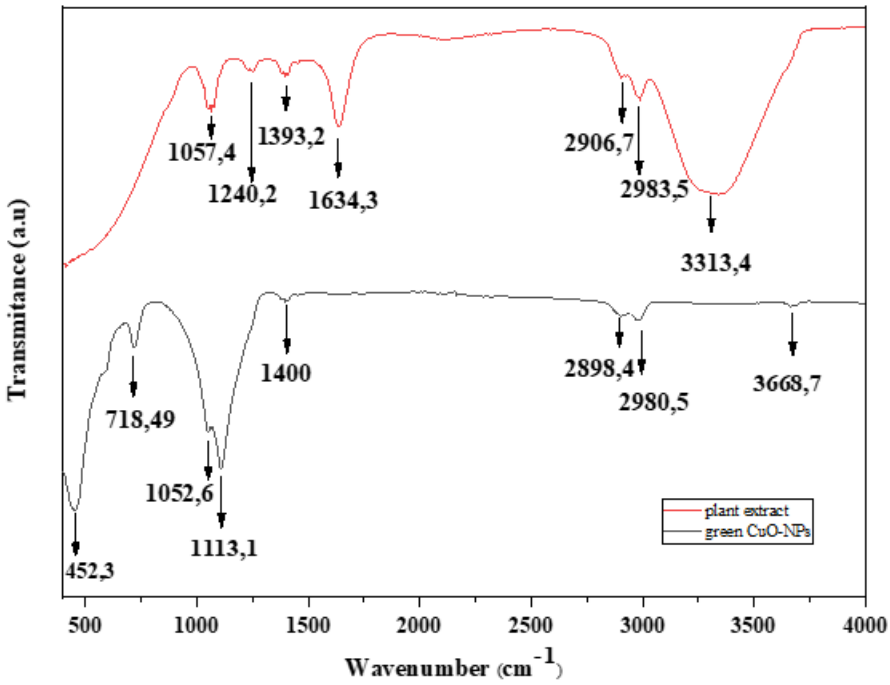

Figure 4

FTIR spectra of biosynthetic CuO NPs

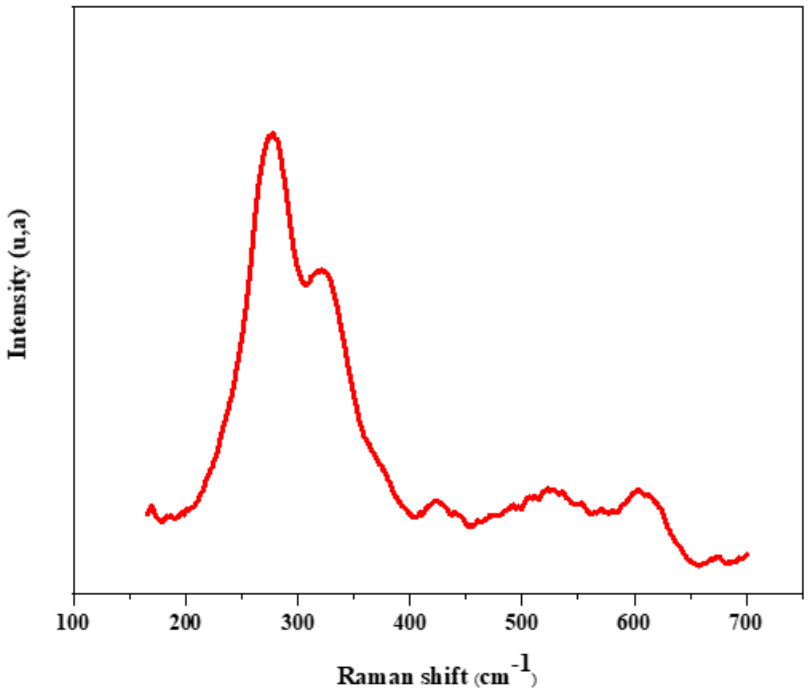

Figure 5

Raman Spectroscopy of CuO-NPs Nanoparticles

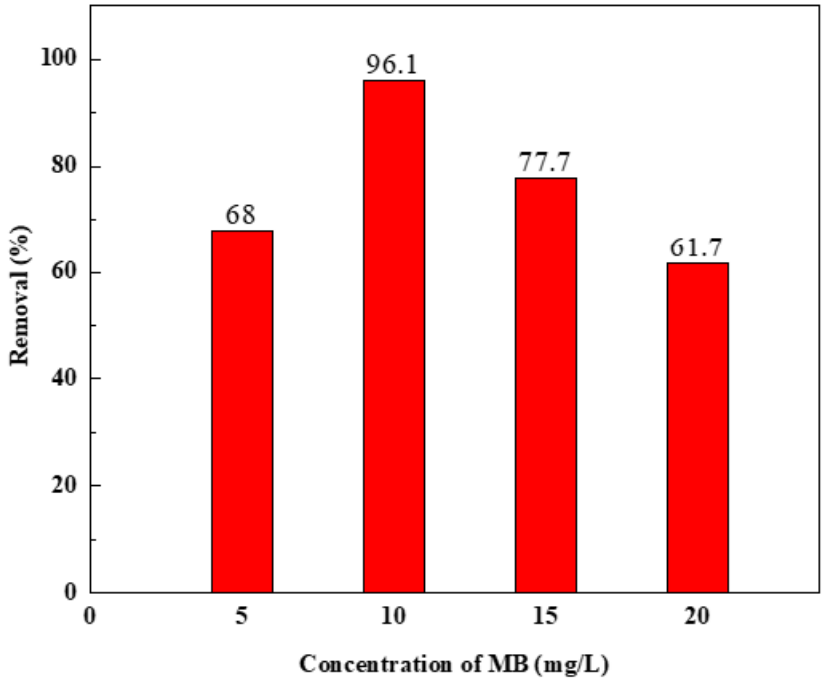

Figure 6

Removal efficiency at different values of MB concentration levels by synthesized CuO NPs

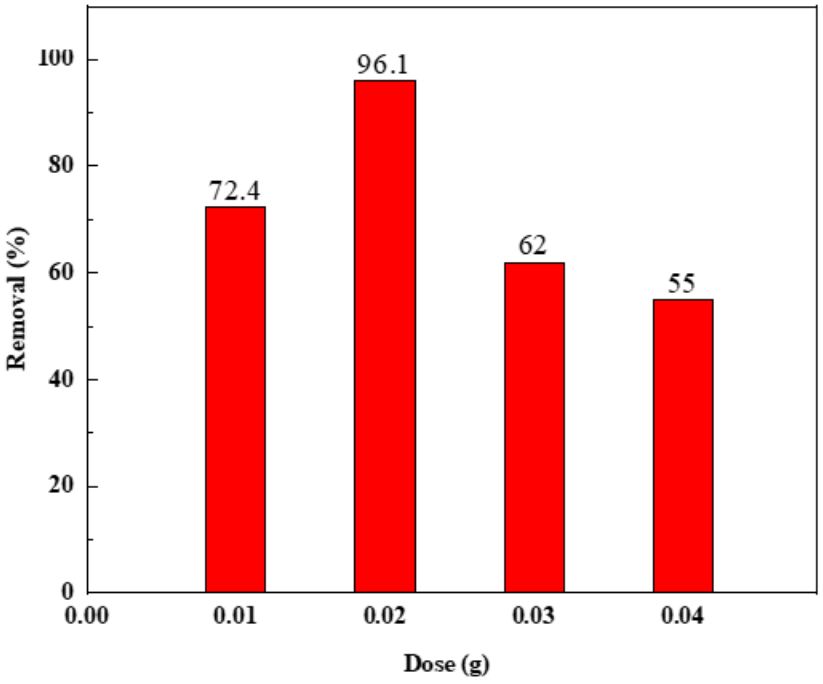

Figure 7

Removal efficiency at different adsorbent dose levels by synthesized CuO NPs

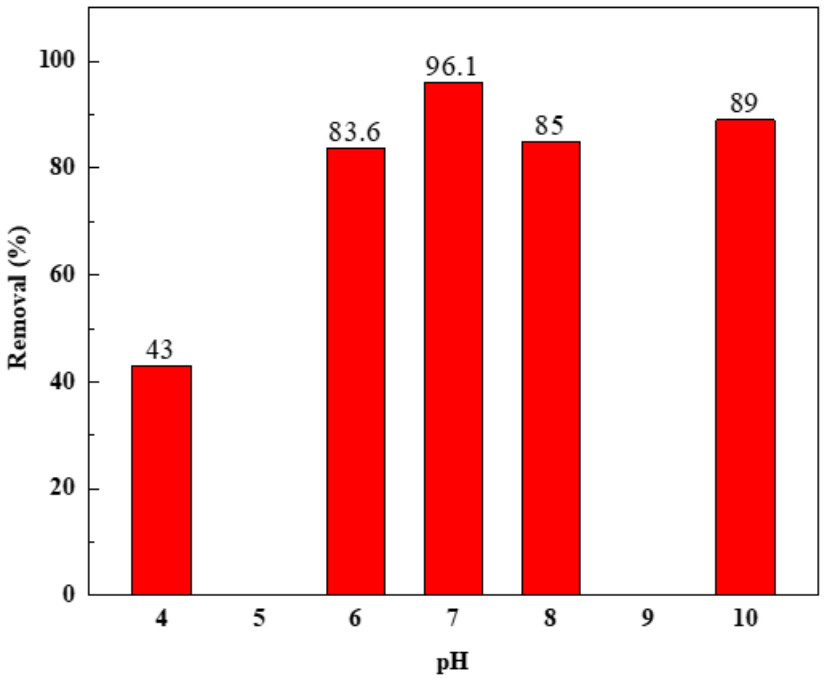

Figure 8

MB removal efficiency at different pH levels by synthesized CuO NPs

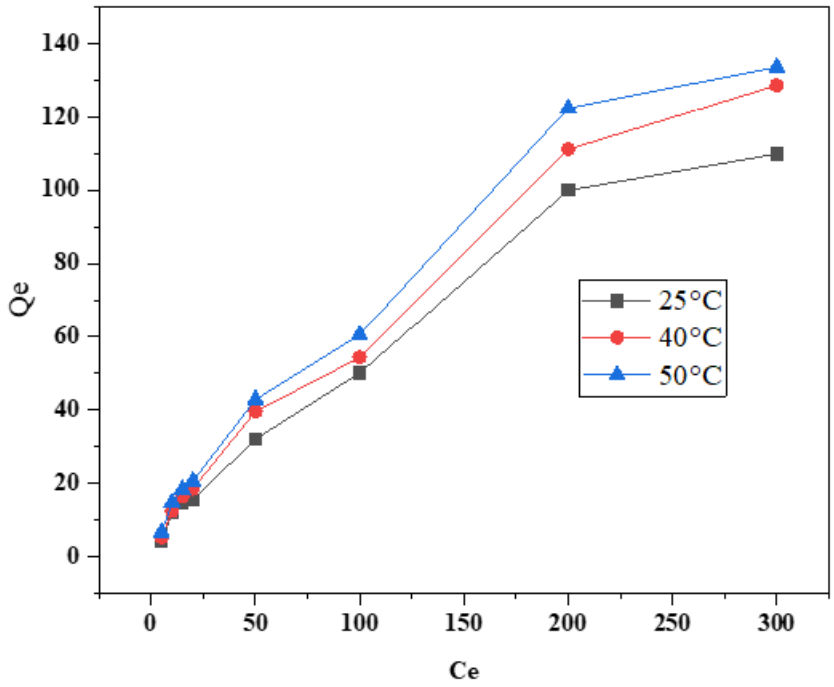

Figure 9

Fig.7 Adsorption capacity of MB on the biosynthesized CuO nanoparticles as a function of equilibrium concentrations at different temperatures

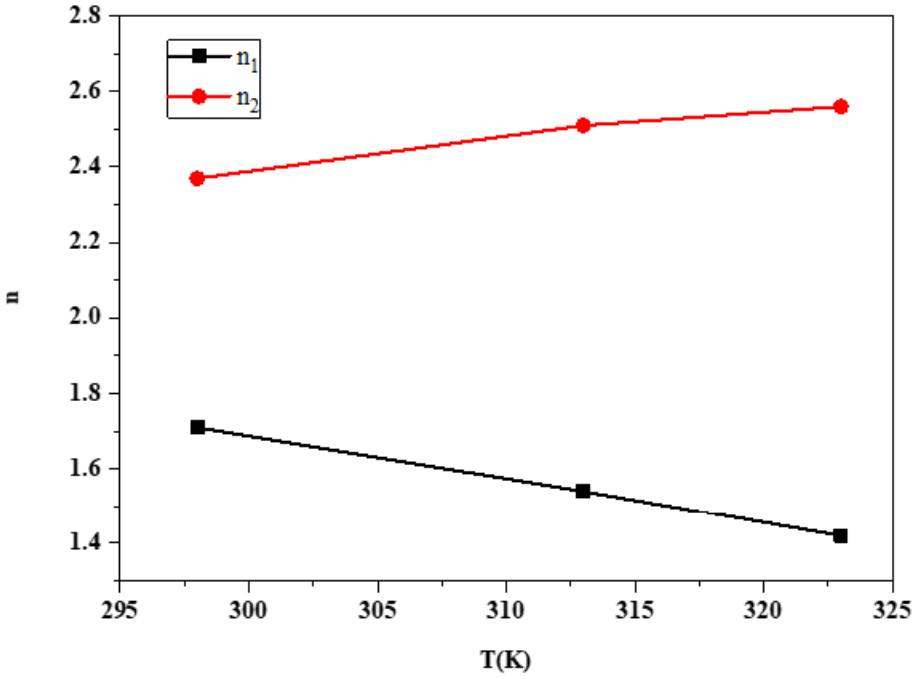

Figure 10

Fig.8 Impact of temperature on the parameter n for the adsorption systems at pH= 7

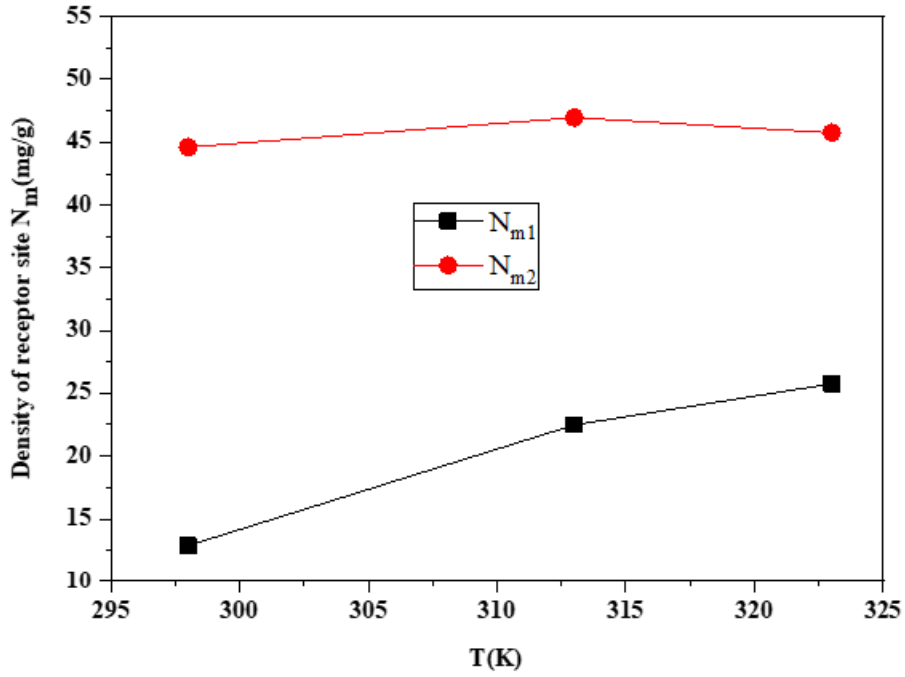

Figure 11

Fig. 9 Effect of temperature on the two densities N_{m1} and N_{m2} for the adsorption systems at pH 7

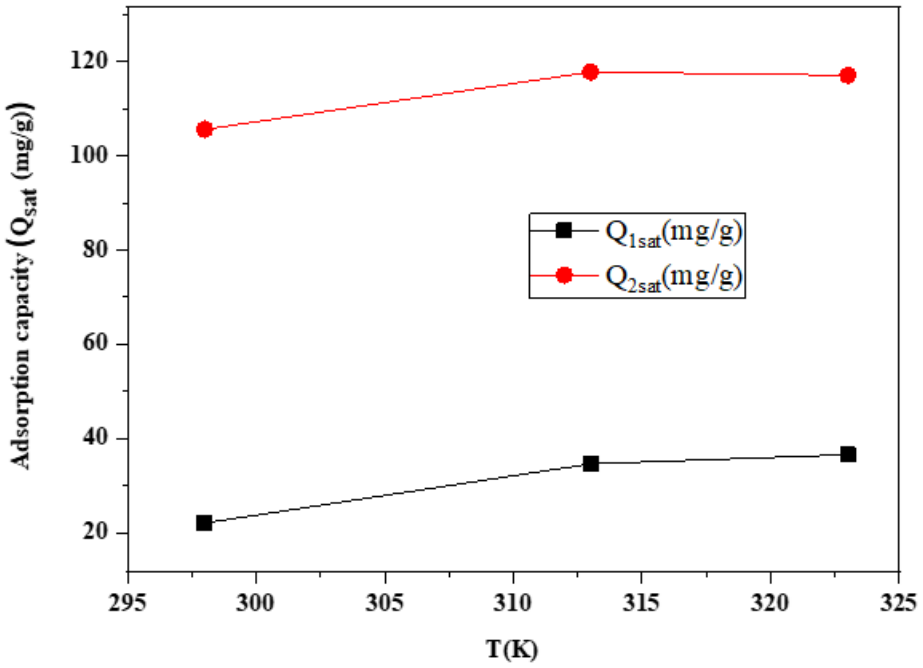

Figure 12

Fig.10 Effect of the temperature on the saturation adsorption capacity for the adsorption systems at pH 7

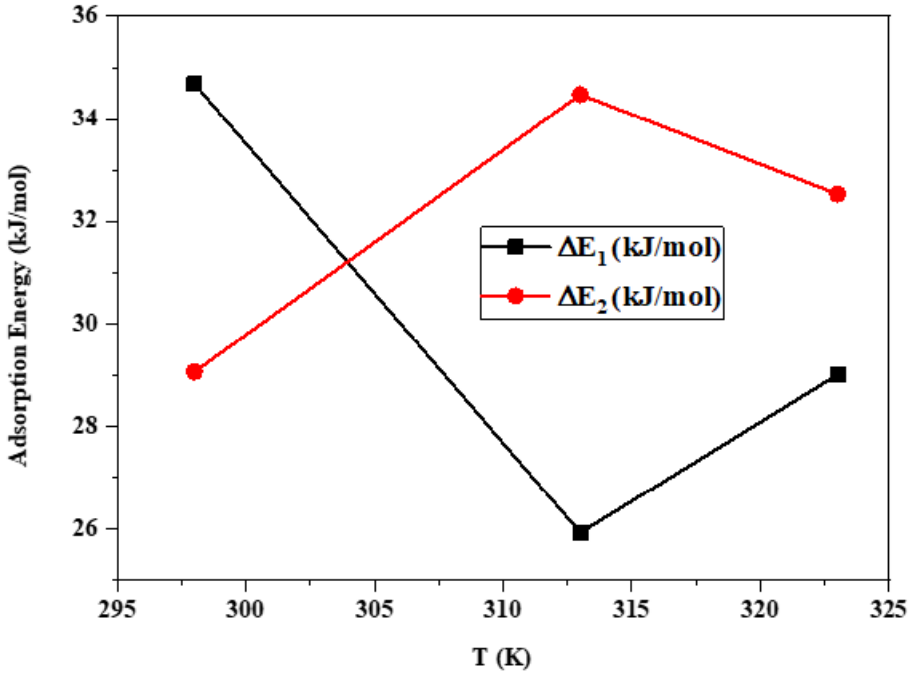

Figure 13

Fig.11 Impact of temperature on the calculated energies for the adsorption systems

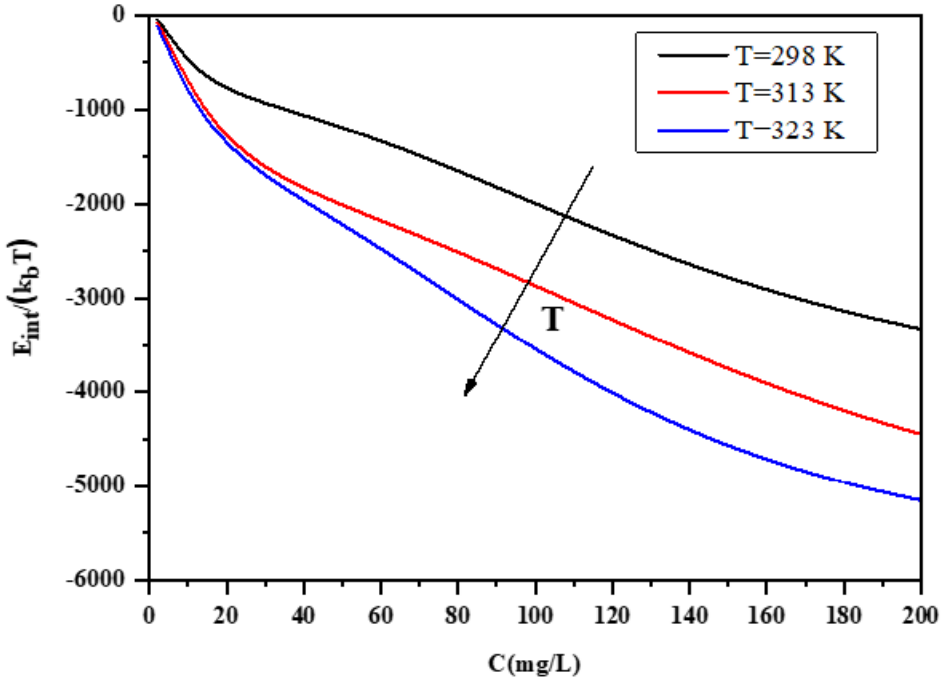

Figure 14

Fig. 12 Evolution of the internal energy versus MB concentration on the surface of the CuO NPs

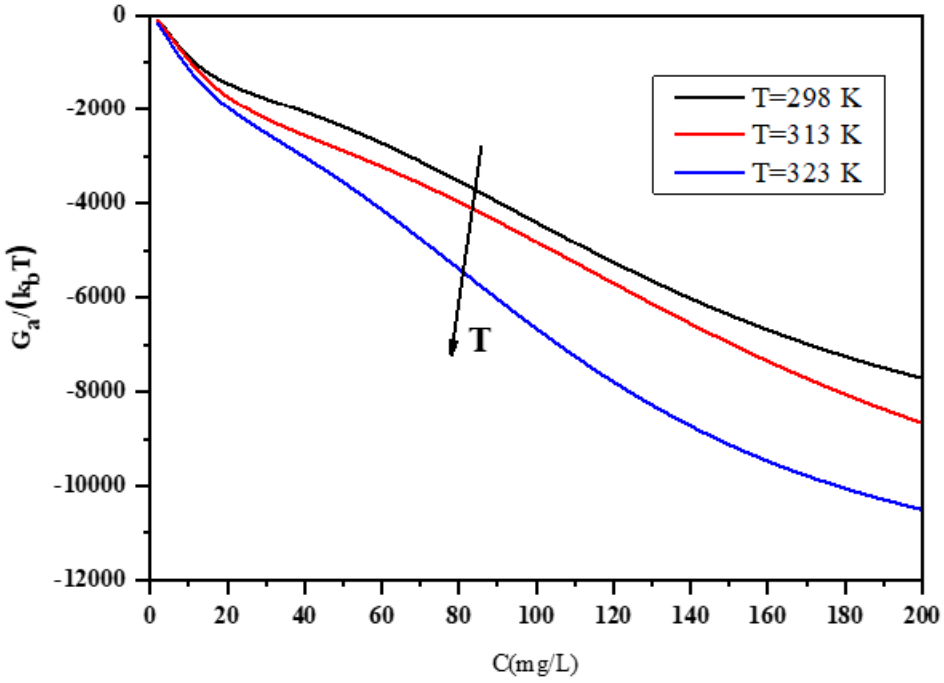

Figure 15

Fig. 13 Evolution of the Gibbs free enthalpy versus MB concentration on the surface of the CuO NPs

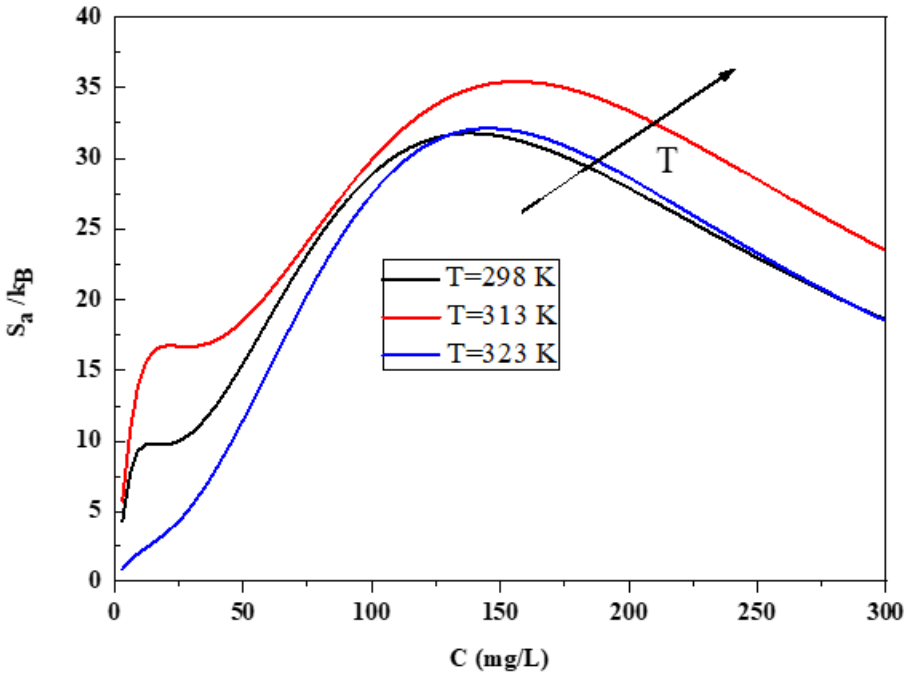

Figure 16

Fig.14 Evolution of the entropy versus MB concentration on the surface of nanoparticles (CuO)

Supplementary Files

This is a list of supplementary files associated with this preprint. Click to download.

- SupplementaryMaterial.docx